Method of oriented circular dichroism

Yili Wu, Huey W. Huang, and Glenn A. Olah
Physics Department, Rice University, Houston, Texas 77251

ABSTRACT We present a new method for determining the orientation of α-helical sections of proteins or peptides in membrane. To apply this method, membranes containing proteins must be prepared in a multilayer array. Circular dichroism (CD) spectra of the multilayer sample are then measured at the normal as well as oblique incident angles with respect to the bilayer planes; we call such spectra oriented circular dichroism (OCD). The procedure of OCD measurement, particularly the ways to avoid the spectral artifacts due to the effects of dielectric interfaces, linear dichroism and birefringence, and the method of data analysis are described in detail. To illustrate the method, we analyze the OCD of alamethicin in diphytanoylphosphatidylcholine multilayers. We conclude unambiguously that the helical section of alamethicin is parallel to the membrane normal when the sample is in the full-hydration state, but the helical section rotates to the plane of membrane when the sample is in a low-hydration state. We also obtained the parallel and perpendicular CD spectra of α-helix, and found them to be in agreement with previous theoretical calculations based on the exciton theory. These spectra are useful for analyzing protein orientations in future experiments.

INTRODUCTION

This paper describes a method of determining the orientation of α-helices embedded in membrane by a novel use of circular dichroic spectroscopy. Its principle is based on the Moffitt theory (Moffitt, 1956; Moffitt et al., 1957) which predicts that one of the peptide transitions in a helix is polarized parallel to the helical axis. For a long time this theory was supported by qualitative results of experiments on partially oriented long α-helical polypeptides. But these experimental supports were called into question by Yamaoka et al. (1986), who measured linear dichroism of electric-field oriented polypeptides. The confusion was, in our opinion, the result of neglecting the bending flexibility of long polypeptide molecules (see Olah and Huang, 1988*b*, for the details). Using a multilayer sample of short helical peptides embedded in membrane and measuring its circular dichroism (CD) at a series of oblique incident angles, we were able to prove unequivocally Moffitt's prediction on polarization (Olah and Huang, 1988*a*). As we will see below, the results presented in this paper further confirm the quantitative details of the theoretical predictions.

Clearly the method we used to prove the Moffitt theory can be used to analyze the orientation of helical sections in membrane proteins. Two experimental procedures are essential for this application. First, the membranes containing proteins are stacked to form a multilayer system, i.e., a L_α lamellar liquid crystal, sandwiched between two quartz plates in which the planes of the stacked bilayers are parallel to the plates. Second, the CD spectra of the multilayers are then measured with the light incident at normal and oblique angles with respect to the planes of the stacked bilayers. It is known that measurement of CD may be distorted by the effects of linear dichroism and linear birefringence, particularly when the multilayer samples are measured at oblique incident angles. It is important to understand these effects and make certain that they are separated from the true CD spectra.

To illustrate the method of oriented circular dichroism (OCD), we present the measurement and analysis of the CD of alamethicin in diphytanoylphosphatidylcholine (DPhPC) multilayers. Alamethicin is a membrane peptide of 20 amino acids. In a membrane environment, whether in a vesicle dispersion or in multilayers, the CD of alamethicin is that of a typical α-helix, although its amplitude indicates that only 40–50% of the residues are in the helical form; the nonhelical part apparently contributes little to the total CD (Nagaraj and Balaram, 1981). Thus, the OCD of alamethicin in membrane reflects the orientation of its α-helical section.

The stable state of hydrated DPhPC at room temperature (~20°C) is the L_α lamellar liquid crystalline phase, in which the lipid molecules are arranged in equally spaced planar bilayers separated by water layers. The water content can be controlled by exposing multilayers to H_2O vapor of chosen partial pressures; it may vary from a high

Address correspondence to Dr. Huang.

0006-3495/90/04/797/10 $2.00

40% (wt/wt) water content to a low 15%; in this hydration range the multilayers remain in the uniaxial L_α phase. By the method of OCD, we found alamethicin molecules mixed in the DPhPC multilayers changing their orientation with the degree of hydration. The significance of this orientation dynamics of alamethicin will be expounded in another paper (Wu, Y., H. W. Huang, and G. A. Olah, manuscript submitted for publication). Here we will concentrate on the details of this new method of circular dichroic spectroscopy.

THEORETICAL BACKGROUND

Let's consider a membrane protein which on average possesses an uniaxial symmetry with the axis denoted by a. The symmetry could be either the intrinsic molecular property or the result of rotational distribution of a large number of molecules around the axis a. Let's denote the direction of propagation of the probing light by k. $G_{//}$ is the molecular CD when k is parallel to a, and $G_\perp$ the molecular CD when k is perpendicular to a. The sample is composed of multilayers of lipid bilayer membrane with the protein molecules embedded in the bilayers. Let the normal to the plane of membrane be n and the angle between n and a be ϕ. In the liquid crystalline L_α phase of the membrane, we assume that the molecular axis a is uniformly distributed over all values of the azimuthal angle around n. The OCD of the sample, $\theta(\alpha)$, is measured at an incident angle α between k and n, and averaged over all values of the azimuthal angle around the beam direction k. The general property of CD gives the following orientation dependence (Tinoco and Hammerle, 1956):

$$\theta(\alpha) = \theta(0°)\cos^2\alpha + \theta(90°)\sin^2\alpha. \quad (1)$$

It is easy to show that

$$\theta(0°) = G_{//}\cos^2\phi + G_\perp\sin^2\phi, \quad (2)$$

$$\theta(90°) = \tfrac{1}{2}G_{//}\sin^2\phi + G_\perp(1 - \tfrac{1}{2}\sin^2\phi). \quad (3)$$

Suppose that two samples are prepared under two different conditions A and B, such that the inclination angle ϕ is changed from ϕ_A to ϕ_B. The OCD for state A and state B give

$$\theta_A(0°) = G_{//}\cos^2\phi_A + G_\perp\sin^2\phi_A, \quad (4)$$

$$\theta_A(90°) = \tfrac{1}{2}G_{//}\sin^2\phi_A + G_\perp(1 - \tfrac{1}{2}\sin^2\phi_A), \quad (5)$$

$$\theta_B(0°) = G_{//}\cos^2\phi_B + G_\perp\sin^2\phi_B, \quad (6)$$

$$\theta_B(90°) = \tfrac{1}{2}G_{//}\sin^2\phi_B + G_\perp(1 - \tfrac{1}{2}\sin^2\phi_B). \quad (7)$$

The four equations are, however, not independent; even if one makes use of two independent CD bands at different wavelengths, it is not possible to determine $G_{//}$, $G_\perp$, ϕ_A, and ϕ_B, unless there is an additional input such as the Moffitt theory. OCD can nevertheless serve a useful purpose even when an additional input is unavailable. If the results of OCD are consistent with Eqs. 4–7, it can be used as a proof that state A and state B are different only by a rotation of the molecular axis, not, for example, different in the secondary structure of the protein.

Another case of interest is that there are two possible orientations for the helix, and state A and state B represent two different distributions of the helices in these two orientations. OCD cannot distinguish a two-orientation problem from a rotation problem. For example, if the two possible orientations are parallel and perpendicular to the normal of membrane and x_A (x_B) represents the fraction of the helices of state A (B) in the parallel orientation, then

$$\theta_A(0°) = x_A G_{//} + (1 - x_A) G_\perp \quad (8)$$

$$\theta_A(90°) = \tfrac{1}{2}(1 - x_A)G_{//} + \tfrac{1}{2}(1 + x_A)G_\perp \quad (9)$$

$$\theta_B(0°) = x_B G_{//} + (1 - x_B) G_\perp \quad (10)$$

$$\theta_B(90°) = \tfrac{1}{2}(1 - x_B)G_{//} + \tfrac{1}{2}(1 + x_B)G_\perp. \quad (11)$$

These equations are equivalent to Eq. 4–7, if we let $x_A = \cos^2\phi_A$, $x_B = \cos^2\phi_B$.

The CD spectra sensitive to the secondary structures of proteins occur below 240 nm. The lower wavelength limitation of commercial CD spectrometers is ~185 nm. Within this range the peptide spectra are dominated by the π–π^* and n–π^* transitions (see a summary of the CD theories in Woody, 1985). The n–π^* transition is characterized by a magnetic dipole transition moment directed along the carbonyl bond, which in a helix gives rise to a negative CD band near 224 nm; the band is approximately Gaussian. The π–π^* transition in a helix splits into three. One has its electric transition dipole polarized parallel to the helical axis and gives rise to a negative Gaussian band near 205 nm. The other two have their electric transition dipoles polarized perpendicular to the helical axis, and their amplitudes strongly depend on the angle between the direction of the probing light and the helical axis (or, more precisely, the projection of the wave vector on the helical axis). When the angle is 0°, these two transitions combine to have the shape of the derivative of a Gaussian centered near 190 nm with the positive amplitude on the long wavelength side, called the helix band (Tinoco, 1964). On the other hand, when the angle is 90°, the two transitions are degenerate, both are positive Gaussians, and are centered near 190 nm. Thus, if the incident light is parallel to the helix axis, its CD is given by

$$G_{//} = \theta_{\pi\to\pi^*}(g_H, 190\text{ nm}, //) + \theta_{n\to\pi^*}(-g, 224\text{ nm}, //), \quad (12)$$

whereas the perpendicular CD is given by

$$G_{\perp} = \theta_{\pi\to\pi^*}(+g, 190\text{ nm}, \perp) + \theta_{\pi\to\pi^*}(-g, 205\text{ nm}, \perp) + \theta_{n\to\pi^*}(-g, 224\text{ nm}, \perp), \quad (13)$$

where in the parentheses, the symbol g or g_H indicates that the band is a Gaussian or the helix form, respectively, and the sign in front of g stands for positive or negative amplitude; the second entry is the wavelength; the third denotes whether the helix is parallel or perpendicular to the light.

EFFECTS OF TILTED INTERFACE, LINEAR DICHROISM, AND LINEAR BIREFRINGENCE

The artifacts in CD spectroscopy have been thoroughly discussed recently by Shindo and Nakagawa (1985) and by Schellman and Jensen (1987; also see the references cited therein). The most serious problems are caused by the coupling of the anisotropic properties of the sample to the nonideal properties of the instrument. The latter include (*a*) anisotropic transmittance in the photodetector, (*b*) a residual static strain birefringence in the photoelastic modulator, and (*c*) a second harmonic response in the lock-in amplifier (Shindo and Nakagawa, 1985). The quantitative expressions for the effects encountered in this experiment are given in the Appendix. In the following we show how we resolved this problem.

The primary concern in an OCD measurement is the linear dichroism (LD) due to tilted dielectric interfaces. We will use a fused silica plate as a substitute sample to study this problem. Let us denote by α the angle between the normal of the plate, n, and the beam direction k, and by β the angle between an axis of the photoelastic modulator and the plane of incidence (the plane defined by n and k). From electrodynamics, we know that the polarization in the plane of incidence is transmitted more than the polarization perpendicular to the plane. Fig. 1 *A* shows the apparent CD of a fused silica plate oriented at $\alpha = 30°, \beta = 45°$. The apparent CD increases with shorter wavelengths because the increasing refractive index of fused silica enhances the effect. At the same α angle but $\beta = -45°$, the apparent CD is equal and opposite in sign to the CD of $\beta = 45°$ (Fig. 1 *C*). No apparent CD was detected when $\beta = 0°$ (Fig. 1 *B*). Indeed we found that at a given wavelength the apparent CD is proportional to sin 2β. Also, as expected, the apparent CD caused by a silica plate is independent of its thickness; a 0.25-mm thick plate and a 3-mm thick plate produced the same spectra shown in Fig. 1.

Eq. A8 in the Appendix describes the total output from the photodetector due to an LD. A numerical estimate

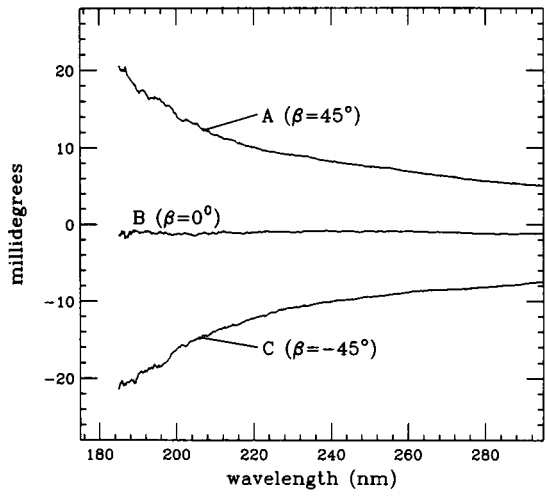

FIGURE 1 Apparent CD due to a tilted fused silica plate. The plate is tilted so that the light is incident at $\alpha = 30°$. The azimuthal angle β (defined in the text and in Fig. 5) is 45° for spectrum A, 0° for spectrum B, and −45° for spectrum C. The spectra are independent of the thickness of the silica plate.

shows that Eq. A8 can be simplified within experimental errors: for a fused silica plate tilted at $\alpha = 30°$ in air, $e^{LD} \sim 1.035$ at wavelength 230 nm (note that this LD is one order of magnitude larger than that of the samples; see below); for our spectropolarimeter (J500-A; Jasco Inc., Easton, MD), $\cos \delta_o \sim 1$, $J_0(\delta_m) \sim 0.32$, or dc(cos) ~ 0.32 (Shindo and Ohmi, 1985); also ΔT was estimated to be ~5% in the range of wavelength 200–300 nm (Shindo and Nakagawa, 1985). Thus, within 1–2% uncertainty the apparent CD is given by Eq. A10, which represents the LD artifact added to the baseline. And after the baseline subtraction the apparent CD is proportional to sin 2β, in agreement with experiment. We note that without the static retardation in the photoelastic modulator and the second harmonic response in the lock-in amplifier, the factor ac(cos) would be zero and LD would not affect CD (this is true for all the cases considered below). However, eliminating only one of these two defects is insufficient to remove the LD effect.

Next we superpose LD on a CD sample. The total output from the photodetector for this case is given by Eq. A11. The magnitudes of CD of our samples are $\sim 10^{-4}$. From the optical rotatory dispersion measurement, we know that CD and circular birefringence (CB) of proteins are of the same order (Imahori and Nicola, 1973). Thus, within 1–2% uncertainty the apparent CD is given by Eq. A12; the spectrum is a linear addition of a CD term and a LD term to the baseline. We tested this by using a tilted silica plate and a solution sample of poly-γ-methyl-L-glutamate (PMLG) which is a typical α-helix former in hexafluoroisopropanol (HFIP). In Fig. 2 we show the CD

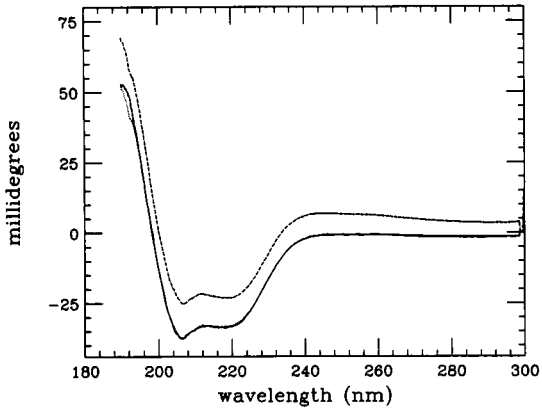

FIGURE 2 CD of a PMLG solution sample with (spectrum A, *dashed line*) and without (spectrum B, *solid line*) a tilted fused silica plate ($\alpha = 30°$) inserted in the light path in front of the PMLG solution. Spectrum C, dotted line, is spectrum A minus the spectrum of the silica plate, Fig. 1 *A*.

spectra of PMLG with (spectrum A) and without (spectrum B) a fused silica plate ($\alpha = 30°, \beta = 45°$) inserted in the light path in front of the sample. (All spectra shown in the figures have their baselines subtracted.) Spectrum C obtained by subtracting the spectrum of the silica plate (Fig. 1 *A*) from spectrum A agrees well with spectrum B. The additivity of LD and CD signals means that LD signal can be removed by averaging over angle β (this averaging method was first suggested by Tunis-Schneider and Maestre, 1970). The factor ac(sin)/[1 + dc(cos) $\Delta T \sin 2a$] multiplying to CD in the first term of Eq. A12 is included in the instrument calibration; its calibrated value is 2, so that in the absence of LD Eq. A12 reduces to CD. Thus LD does not affect the amplitude of CD. The main effect of LD is that in Eq. A12 the LD term can be much larger than the CD term; if the removal of the LD signal from the apparent CD is incomplete, a remaining small fraction of LD signal can still significantly distort the CD spectrum. In practice, we found that the average of the apparent CD measured at 16 equally spaced β angles (0, 22.5°, . . .) effectively eliminates the LD artifact.

We now turn to our OCD samples, which are multilayer membranes sandwiched between two fused silica plates. The anisotropy now includes linear birefringence (LB), LD as well as CD. The main cause of LD is still the tilted dielectric interfaces. To make the LD as small as possible, we have built a sample chamber to minimize the interfacial effect by matching the refractive index along the light path; as a result, we have $e^{LD} = 1.004$ at wavelength 230 nm and $\alpha = 40°$, the largest tilt angle in our OCD measurement (see the experimental section). The LB in our samples is due to the uniaxial nature of membranes. The birefringence (Δn) of multilayers can be measured by conoscopy; we found $\Delta n = 0.031$ for pure lecithin and 0.024 for lecithin containing gramicidin (40 to 1 molar ratio) at wavelength $\lambda = 632.8$ nm (Huang and Olah, 1987); we expect these Δn's to increase by 10% at $\lambda = 200$ nm as Δn of quartz does; we will use $\Delta n = 0.03$ to estimate the LB effect. It is easy to show that when light passes through a stack of bilayers of total thickness D at angle α (with respect to the normal of the membranes), the phase difference between the ordinary and the extraordinary waves is $LB = 2\pi D \Delta n \sin^2 \alpha/\lambda \cos \alpha$ (Born and Wolf, 1980). The largest LB in our OCD measurement is ~15° ($D = 0.5\ \mu m, \alpha = 40°, \lambda = 200$ nm). We will show below that the effect of LB is expressed as 1-cos LB; we see that this factor is at most 0.03 for our samples. The total effect of anisotropy will be estimated by considering a combination of $LD_1 + LB + CD + CB + LD_2$. The optical axes of LD and LB are the same, both defined by the angle β given above.

The result is given in the Appendix, Eqs. A16–18. The apparent CD consists of two parts. One part, $(I_{ac}/I_{dc})_2$, can be removed by averaging over β like the LD term in Eq. A12. The remaining part, $(I_{ac}/I_{dc})_1$, is the CD signal plus the baseline, but both are slightly modified by the LB effect. The size of the baseline is typically 10% or less of the CD signal; therefore, a maximum 3% modification on the baseline is negligible. The factor cos LB multiplying to CD (in Eq. A17) is the only artifact that is not correctable by a simple procedure. However, as we pointed out $1 \geq \cos LB \geq 0.97$, the maximum error is 3%.

To be certain that our β-averaging process indeed removes the β-dependent terms and that the LB effect does not affect our spectra, we run the following test for each OCD spectrum. For each spectrum, we measure the sample alone and measure it again with a PMLG solution sample inserted between the sample and the photodetector. The difference of these two spectra must agree with the PMLG spectrum. Fig. 3 shows the result of the test for the worst case of LB and LD, i.e., for $\alpha = 40°$. Spectrum A is the spectrum of PMLG alone; spectrum B is the difference spectrum, i.e., the spectrum of the combination of an alamethicin/DPhPC multilayer sample ($\alpha = 40°$) and a PMLG solution minus the spectrum of the sample alone, each independently averaged over β. The good agreement shown in Fig. 3 (note that the scale is magnified ten times compared with Fig. 2 and the noise is partly due to the fact that the PMLG solution is diluted for this measurement so that its amplitude is comparable to that of the multilayer sample; see figure caption) indicates that our averaging method correctly removes the spurious effects of a tilted multilayer sample from its CD spectrum.

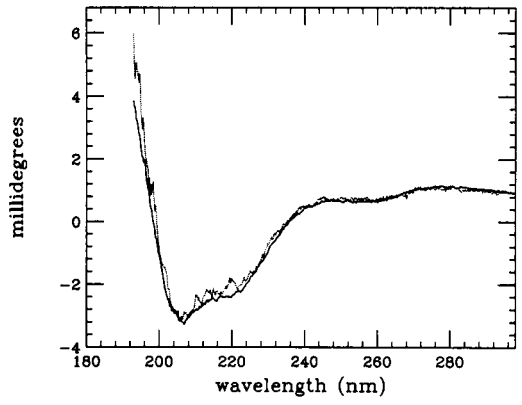

FIGURE 3 To prove that the artifacts of LD and LB are removable by our averaging method, we measured the CD of a tilted (α = 40°) alamethicin/DPhPC multilayer sample with and without a PMLG solution inserted in the light path behind the sample, and each was averaged over β. The latter spectrum was then subtracted from the former to yield spectrum B, the dotted line. This is compared with the CD of the PMLG solution alone (spectrum A, *solid line*). The spectra look noisier than Fig. 2, because the scale is magnified ~10 times and because Fig. 3 was measured at a higher sensitivity level than Fig. 2.

EXPERIMENT

Sample preparation

DPhPC in $CHCl_3$ (20 mg/ml) was purchased from Avanti Polar Lipids, Inc., Pelham, AL. It was further diluted to give a stock solution of 10 mg/ml. Alamethicin was purchased from Sigma Chemical Co., St. Louis, MO; it was used without further purification. A stock solution of alamethicin was prepared in $CHCl_3$:CH_3OH (1:1) at the concentration of 1 mg/ml, and stored at −20°C. For each sample batch, 10 ml of DPhPC stock solution was mixed with the appropriate amount of alamethicin stock solution at the desired molar ratio. A clean nitrogen stream was blown on the solution so as to remove the solvent; then it was further dried under vacuum (10 μm) for 4 h. Approximately 10 ml of distilled water was added to the dry mixture. The mixture was homogenized so as to break up any large aggregates.

A small amount of this homogenized dispersion was removed to prepare a vesicle sample: the allotment was diluted with water to ~1 mg/ml DPhPC concentration, and sonicated for 30 min at 0°C. Immediately after sonication the CD was measured using a 1-mm path length cuvette. To check the effect of light scattering from this particulate system, the CD measurement was performed at two different sample positions from the photodetector; no difference was noticed between these two measurements. The pH of the vesicle dispersion was 6.0–6.4. The concentration of DPhPC in the vesicle sample was rechecked later by using a modified Fiske-SubbaRow method (Dittmer and Wells, 1969). The vesicle sample represents the case where the α-helices are isotropically oriented. When the OCD of a multilayer sample is (mathematically) averaged over all orientations, it should be the same as the vesicle spectrum; thus, the latter serves the purpose of a consistency check.

Multilayer samples were prepared as described by Huang and Olah (1987). The lipid/alamethicin dispersion was sonicated, lyophilized, and left under vacuum for 24 h. The fluffy powder was removed from vacuum and placed in a container, which was placed in a larger flask containing a small amount of water. The flask was then sealed and placed in the dark. The top of the sample container was left open so the sample would be in contact with H_2O vapor. The sample was incubated for 3–5 d at high humidity (>95%) and room temperature until it appeared to be a clear gel.

Three sample batches, DPhPC/alamethicin at molar ratio 47:1 and 90:1, and pure DPhPC, were prepared by the same procedure. A small amount from each sample batch was then sandwiched between two fused silica plates (1 in × 1 in × 0.5 mm) without a spacer. We were able to align each sample into uniform multilayers within a few minutes (Huang and Olah, 1987). There was no smectic defect as shown under a polarized microscope. Because no spacer was used, the sample thicknesses were ill-defined. Therefore, a duplicate sample with a spacer of known thickness (13 μm) was made. The thickness of the no-spacer sample was determined by the ratio of its CD spectrum to that of the 13-μm-thick sample. (Due to the strong absorption by DPhPC, the measurable spectra of 13-μm-thick samples were limited to above 224 nm.) The thicknesses of the thin samples were ~0.5 μm with less than 10% uncertainty.

PMLG (Mw = 150,000) was purchased from Sigma Chemical Co. and was used without further purification. HFIP was purchased from Aldrich Chemical Co., Milwaukee, WI; it was spectroscopic grade. The concentration of PMLG in HFIP was adjusted so that its CD spectrum was about the same order of magnitude as that of the multilayer samples.

Hydration–Dehydration

The multilayer samples were kept in a dark bottle which contains a small amount of water so that the sample was in contact with H_2O vapor through the gap between the two silica plates. The sample in equilibrium with 100% relative humidity (~20°C) has a stable CD spectrum

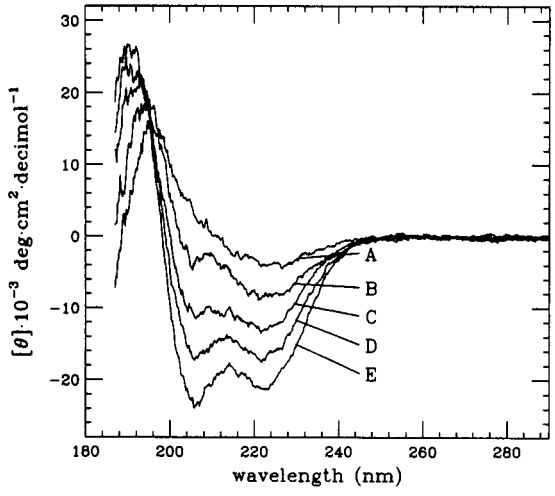

FIGURE 4 CD of alamethicin in DPhPC multilayers as a function of the water content. All spectra were measured at the normal incident angle α = 0°. Spectrum A is the CD of the full-hydration state equilibrated with 100% relative humidity at ~20°. If the sample is exposed to 50% relative humidity, the spectrum changes from A to E through B, C, D. If the sample with spectrum E is exposed to 100% relative humidity, it changes to A through D, C, B. The hydration/dehydration processes are completely reversible.

unchanging in time. This sample is called a fully hydrated sample and its state the full-hydration state. When a fully hydrated sample was exposed to air (50% humidity, 20°C), its CD spectrum underwent dramatic changes during the time course of dehydration and approached a definite CD spectrum, which was stable on further dehydration (Fig. 4). The sample was examined under a polarized microscope during the time course, and no visible change was noticed. This steady state which was reached by dehydration while the multilayers were maintained in the L_α phase is called the low-hydration state. The dehydration process is entirely reversible. When a low-hydration sample was returned to the bottle with 100% relative humidity, its CD spectrum went through the transient states seen during dehydration in the reversed order, and approached the full-hydration state. In general the dehydration process from the full- to the low-hydration state takes ~3–4 d, whereas the hydration process takes ~4 d. If a sample was kept in air longer than 5–7 d, smectic defects began to appear near the edge. Unless the defects were severe, the sample recovered upon hydration.

For the purpose of subtracting the lipid background from the CD of alamethicin in multilayers, a pure DPhPC sample was prepared for each alamethicin sample by the identical procedure, and the pair were always kept in the same hydration condition. We found little changes in the CD of pure DPhPC during the dehydration or the hydration process. The 13-μm-thick samples, which were prepared for the purpose of determining the thicknesses of the thin samples, behaved exactly like the thin samples. The thickness normalization was performed in the full- and low-hydration state separately. The normalization ratios obtained in these two ways agree within 10%.

CD measurement

Circular dichroism spectra were measured on a spectropolarimeter (J500-A; JASCO). 0.06% (w/v) ammonium d-camphor-10 sulfonate in H_2O was used to calibrate the CD scale assuming a molar ellipticity of $[\theta]_{290.5\,nm} = +7895.1$ deg · cm^2/dmol. The wavelength was calibrated with the 586-nm peak of neodymium glass and the 287.7-nm peak of holmium glass. A computer-controlled rotator was mounted in the CD sample compartment as described by Olah and Huang, 1988*a*. The rotator's axis was collimated with the light beam.

One way to reduce the LD effect, that is discussed in a previous section, is to make the dielectric discontinuities on the tilted interfaces as small as possible. In the previous experiment (Olah and Huang, 1988*a*), we cut a fused silica cylinder into two at a desired tilt angle and inserted a multilayer sample between them, so that the light passed through the tilted sample practically without refraction. However, the alignment procedure for this sample assembly is tedious and time-consuming. In the present experiment, we used a different sample assembly to achieve the same purpose. A hollow aluminum cylinder was built with each end sealed by a plane silica window, and with an opening on the side. A multilayer sample in silica plates was sealed with apiezon W wax around its edge before it was positioned and fixed inside the cylinder with its normal making a chosen angle with the cylindrical axis (Fig. 5). The interior was then filled with distilled water, and the side opening covered and sealed. The cylinder/sample assembly was mounted on the rotator mentioned earlier, which allowed the assembly to be rotated about the cylindrical axis. By this arrangement the light enters and emerges from the high refractive index region both by normal incidence. Inside the cylinder, water diminishes the variation of the refractive index along the light path, so that the effect of interfaces discussed above are reduced. The refractive index of hydrated DPhPC at 589.3 nm and 486.1 nm was measured on an Abbe refractometer, and its wave-length dependence was estimated by using the Sellmeier equation (Fasman, 1974); its value varies from 1.45 at 486 nm to 1.56 at 199 nm. The angles of refraction in DPhPC when light from water incident on the silica surface at 30° and 45° were calculated by using Snell's law. The variations of the angles of refraction with wavelength from 195 to 260 nm are <0.5%, which is within the error of our angle measurement. Therefore, the angles are approximately independent of the wavelength. When the sample is tilted at 30°, the angle α between the normal of the sample plane and the light beam actually passing through the lipid multilayers is 27°; when the sample is tilted at 45° the angle α is 40° (Fig. 5).

A single spectrum was the average of 16 scans which correspond to 16 angles of β (0°, 22.5°, 45°, . . . , 337.5°). The background of the water chamber was measured and subtracted from each spectrum.

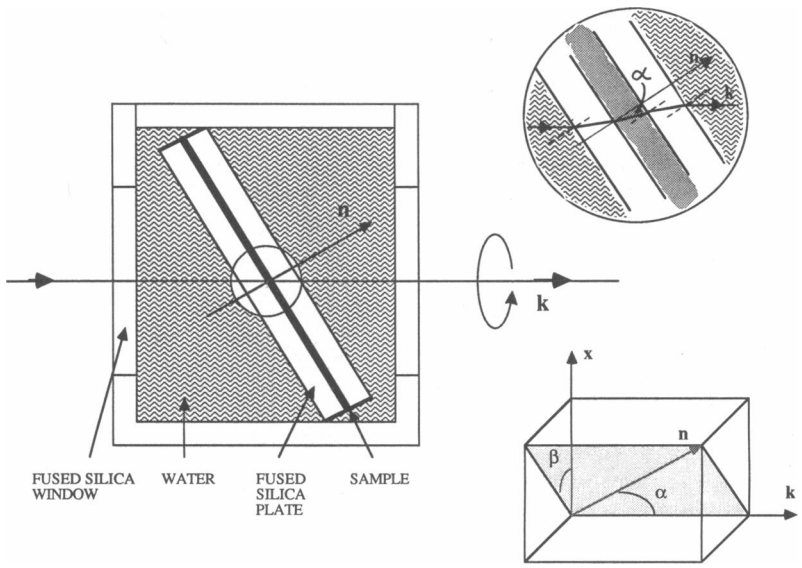

FIGURE 5 Schematic drawing of the sample chamber. The part of the diagram inside the circle is magnified to show the angle α. β is the angle between the phase-retardation axis of the photoelastic modulator, x, and the plane of incidence defined by k and n.

DATA ANALYSIS AND DISCUSSIONS

Fig. 6 shows two sets of OCD spectra obtained from one alamethicin multilayer sample in the full-hydration state, spectrum A, B, C, and in the low-hydration state, spectrum D, E, F (the corresponding lipid background has been subtracted from each spectrum). Although in each set of OCD only two spectra are independent, it is a good practice to measure spectra at more than two angles. The consistency check of the tilt angle dependence by Eq. 1 often serves to screen the suspect data.

Next, one may assume a value for x_A ($\cos^2 \phi_A$), and solve for $G_{//}$, $G_\perp$ by using Eqs. 8–9 and also solve for x_B ($\cos^2 \phi_B$) by using

$$[\theta_A(0°) - \theta_A(90°)]x_B = \tfrac{1}{2}[\theta_A(0°) - \theta_B(0°)] + [\tfrac{3}{2}\theta_B(0°) - \tfrac{1}{2}\theta_A(0°) - \theta_A(90°)]x_A. \quad (14)$$

The last equation is obtained by eliminating $G_{//}$ and $G_\perp$ from Eqs. 8–10. Now if $G_{//}$, $G_\perp$, and x_B so obtained would satisfy Eq. 11 as it does in our case, then we have proven that state A (full-hydration state) and state B (low-hydration state) are related to one another either by a rotation of the molecular axis or as two different mixing states of two possible helical orientations. The value one assumes for x_A for this part of analysis is totally arbitrary. One purpose of this paper is to provide the experimentally determined $G_{//}$ and $G_\perp$ for α-helices, so that for future experiments one can determine the inclination angle ϕ of α-helix by directly using Eq. 2 (or determine the fraction x_A by using Eq. 8).

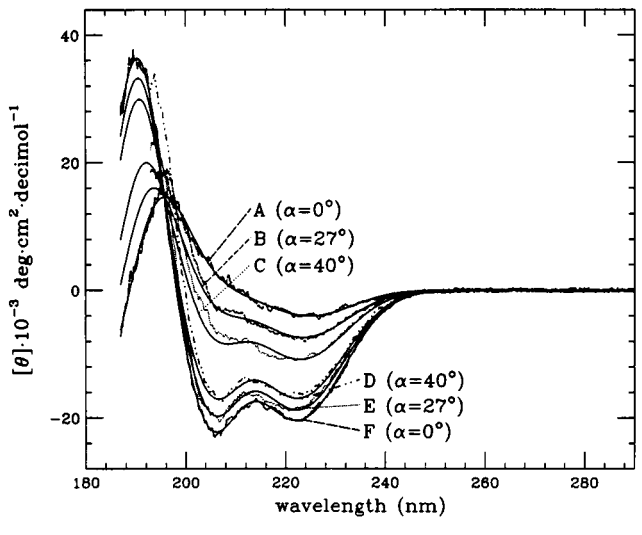

FIGURE 6 OCD of alamethicin in DPhPC multilayers in the full-hydration state (A, B, C) and in the low-hydration state (D, E, F). The solid lines for A and F are the least-squares fits. The solid lines for B, C, D, E are constructed from A and F by using Eqs. 1–3.

Moffitt's theory predicts that the negative CD band near 205 nm consists of $G_\perp$ component only, i.e., $G_{//} = 0$ for this band. Consequently, we expect the CD amplitude near 205 nm to obey the following α-dependence,

$$\theta(\alpha) = G_\perp[\sin^2 \phi + (1 - \tfrac{3}{2}\sin^2 \phi)\sin^2 \alpha]. \quad (15)$$

In particular, for helices parallel to the membrane normal ($\phi = 0°$) one has $\theta(\alpha)$ increasing with $\sin^2 \alpha$, whereas for helices perpendicular to the membrane normal ($\phi = 90°$) $\theta(\alpha)$ decreasing with $\sin^2 \alpha$. Thus a visual inspection of the OCD (Fig. 6) is sufficient to conclude that the inclination angle ϕ must be small for the full-hydration state and large for the low-hydration state. Indeed, if we let x_A(or $\cos^2 \phi_A$) equal to one, i.e., $\phi_A = 0°$, Eq. 14 yields x_B (or $\cos^2 \phi_B$) equal to zero, or $\phi_B = 90°$.

A nonlinear least-squares program was written to fit the phenomenological expressions Eqs. 12 and 13 to the spectra of normal incidence ($\alpha = 0°$). Each Gaussian band is assumed to have a form

$$g = A \exp[-(\lambda - \lambda_0)^2/\Delta^2] \quad (16)$$

with three parameters: A the amplitude, λ_0 the peak position, and Δ the band width. The helix band has the form (Tinoco, 1964)

$$g_H = A[2(\lambda - \lambda_0)(\lambda_0/\Delta^2) + 1] \exp[-(\lambda - \lambda_0)^2/\Delta^2] \quad (17)$$

also with three parameters. Spectrum F of the low-hydration state fits very well (see Fig. 7) with three Gaussian bands as prescribed by the theory (Eq. 13) for helices perpendicular to the light. On the other band, spectrum A of the full-hydration state would not fit well with a combination of Gaussian bands, instead it fits a combination of a Gaussian and a helix band (see Fig. 8), exactly as predicted by the Moffitt theory (Eq. 12) for helices parallel to the light. The band parameters obtained from our fit (Table 1) are in good agreement

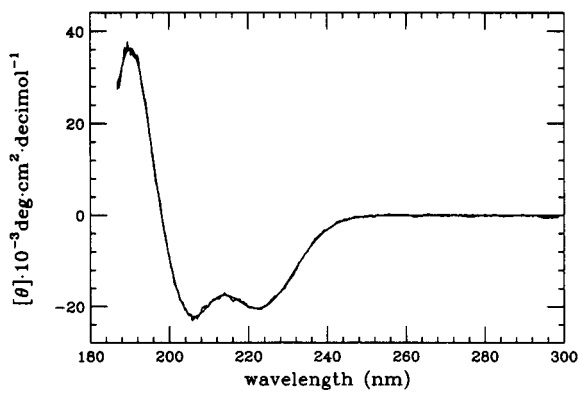

FIGURE 7 Spectrum F of Fig. 6 is fitted with Eq. 13. The band parameters are given in Table 1.

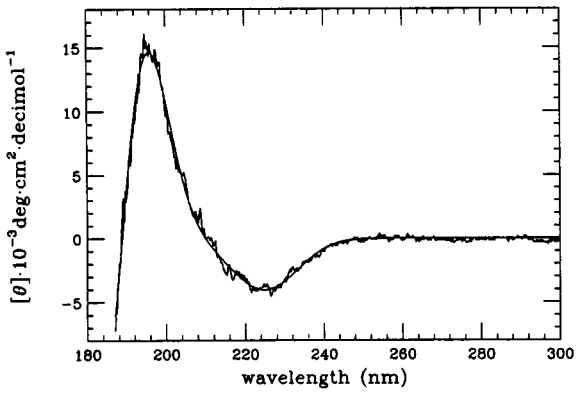

FIGURE 8 Spectrum A of Fig. 6 is fitted with Eq. 12. The band parameters are given in Table 1.

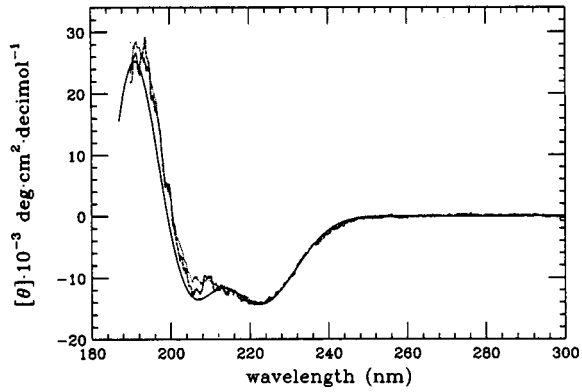

FIGURE 9 CD of alamethicin in DPhPC vesicles. Solid line is the construction (Eq. 18) from the spectra of the multilayer sample. Dashed line is the measured spectrum of vesicles with 100:1 lipid to peptide ratio, and dotted line that of 50:1 ratio.

with the calculated values given by Woody (1968) and also with the experimental values obtained by Mandel and Holzwarth (1972) from analyzing the spectra of helical polypeptides in solution. With the spectrum A designated for $G_{//}$ and the spectrum F designated for $G_{\perp}$, we use Eqs. 1–3 to construct the spectra for $\phi_A = 0°$ at $\alpha = 27°$ and 40°, and for $\phi_B = 90°$ at $\alpha = 27°$ and 40°; they agree with spectrum B, C, E, D of Fig. 6, respectively (see below). Also the transient spectra obtained between the full- and low-hydration states (Fig. 4) can each be fitted very well with a linear combination of spectrum A and spectrum F, indicating that they are mixed states. (From the OCD alone, we cannot exclude the possibility that a transient state is a state of inclined helices with ϕ between 0° and 90°, but physically this is unlikely.)

Finally, we can also compare the OCD of a multilayer sample with the CD of a vesicle sample. Because the orientation of α-helix is isotropically distributed in a vesicle sample, we have the vesicle spectrum related to $G_{//}$ and $G_{\perp}$ by

$$\theta_v = \tfrac{1}{3}G_{//} + \tfrac{2}{3}G_{\perp}. \quad (18)$$

The spectrum constructed from $G_{//}$ and $G_{\perp}$ agrees with the measured vesicle spectrum except that the vesicle spectrum is slightly red shifted near 200 nm (Fig. 9). A similar red shift is also noted for measured spectra B, C, D, E in Fig. 6 compared with their respective constructed spectra. We suspect that this could be due to the small contribution from the nonhelical part of alamethicin, which may rotate differently from the helical section when the hydration condition changes.

In conclusion, we have shown, by the use of OCD, that the helical section of alamethicin changes from an orientation parallel to the membrane normal in the full-hydration state to an orientation perpendicular to the membrane normal in the low-hydration state. By this analysis we have obtained $G_{//}$ and $G_{\perp}$ of α-helix, the two basic components of the orientation-dependent spectrum; they can be used for the orientation analyses of membrane proteins in future experiments.

APPENDIX

Artifacts in OCD measurement

The notations used below are similar to, but not exactly the same as, that of Shindo and Nakagawa (1985). In a typical CD spectrometer, a

TABLE 1 Band parameters for CD of α-helix

CD band		Band center	Band width	Amplitude of alamethicin	Amplitude of α-helix‡
		λnm	Δnm	$A\ 10^{-3}\ deg\ cm^2\ decimol^{-1}$	$A\ 10^{-3}\ deg\ cm^2\ decimol^{-1}$
$n \rightarrow \pi^*$,	helix $\perp$ $k(g)$*	222.3	12.9	−20.37	−51
	helix//$k(g)$	224.9	11.9	−4.04	−10
$\pi \rightarrow \pi^*$,	helix $\perp$ $k(g)$	204.8	7.4	−18.65	−46
$\pi \rightarrow \pi^*$,	helix $\perp$ $k(g)$	190.4	6.4	36.73	92
	helix//$k(g_H)$	188.5	10.1	−0.95	−2.4

*g stands for a Gaussian band; g_H for a helix band.

‡The mean residue ellipticity of PMLG in HFIP solution is used as the standard CD for isotropically distributed α-helices. The CD of alamethicin in vesicles is compared with the standard, from which we estimate that 40% of the residues of alamethicin are helical. The numbers on the fifth column are the numbers on the fourth divided by 40%.

linearly polarized light passes through a photoelastic modulator and then through a sample compartment, and enters a photodetector connected to a lock-in amplifier. The principal axes of the modulator are set at 45° to the incident polarization; the modulator provides a phase retardation δ along one axis (this axis is designated X-axis). Ideally the phase retardation should be a pure sinusoidal function of time of the form $\delta_m \sin \omega t$, but it may also contain a static retardation δ_o produced by ambient strain in the modulator. Thus the total phase retardation is $\delta = \delta_o + \delta_m \sin \omega t$, where ω is the fundamental frequency of the modulator, usually 50 kHz. The lock-in amplifier is tuned to the fundamental frequency, but it may still have a second harmonic (100 kHz) response, which will be denoted by $R(2\omega)$. The anisotropic response of the photodetector is expressed by different transmittances T_1 and T_2 in two principal axes, with axis 1 at angle a from X-axis. The output of the spectrometer is the ratio of the ac (50 kHz) to dc signals I_{ac}/I_{dc}, which can be calculated by using the elementary principles of optics (Velluz et al., 1965). For simplicity, we express the dc and ac outputs of cos δ and sin δ from the lock-in amplifier as

$$\cos \delta = \mathrm{dc(cos)} + \mathrm{ac(cos)}, \tag{A1}$$

$$\sin \delta = \mathrm{dc(sin)} + \mathrm{ac(sin)}, \tag{A2}$$

$$\mathrm{dc(cos)} = \cos \delta_o J_0(\delta_m), \tag{A3}$$

$$\mathrm{dc(sin)} = \sin \delta_o J_0(\delta_m), \tag{A4}$$

$$\mathrm{ac(cos)} = 2 \cos \delta_o J_2(\delta_m) R(2\omega) - 2 \sin \delta_o J_1(\delta_m) \sin \omega t, \tag{A5}$$

$$\mathrm{ac(sin)} = 2 \sin \delta_o J_2(\delta_m) R(2\omega) + 2 \cos \delta_o J_1(\delta_m) \sin \omega t, \tag{A6}$$

where J_0, J_1, J_2 are Bessel function of order 1, 2, 3 (Shindo and Nagakawa, 1985). In the absence of any sample, the above described instrument will produce an apparent CD given by

$$I_{ac}/I_{dc} = \text{baseline} = \mathrm{ac(cos)}\Delta T \sin 2a/[1 + \mathrm{dc(cos)}\Delta T \sin 2a], \tag{A7}$$

where $\Delta T = (T_1 - T_2)/(T_1 + T_2)$. This is the baseline.

A sample of linear dichroism (LD) with its principal axis of higher transmittance making an angle β with X-axis produces a total photodetector output

$$\begin{aligned} I(\mathrm{LD}) = I_{ac} + I_{dc} &= 1 + \cos \delta \sin 2\beta (e^{\mathrm{LD}} - 1)/(e^{\mathrm{LD}} + 1) \\ &+ \Delta T[\cos 2(a - \beta)(e^{\mathrm{LD}} - 1)/(e^{\mathrm{LD}} + 1) \\ &+ \cos \delta \sin 2\beta \cos 2(a - \beta) \\ &+ \cos \delta \cos 2\beta \sin 2(a - \beta) 2e^{\mathrm{LD}/2}/(e^{\mathrm{LD}} + 1)], \end{aligned} \tag{A8}$$

where a proportionality constant common to both I_{dc} and I_{ac} is omitted. In all the cases under consideration, we have $1 < e^{\mathrm{LD}} < 1.04$. Hence we have $(e^{\mathrm{LD}} - 1)/(e^{\mathrm{LD}} + 1) \sim \mathrm{LD}/2$, $2e^{\mathrm{LD}/2}/(e^{\mathrm{LD}} + 1) \sim 1$, and I_{ac}/I_{dc} as follows

$$\begin{aligned} I_{ac}/I_{dc} = [&\mathrm{ac(cos)}\ (\mathrm{LD}/2) \sin 2\beta \\ &+ \mathrm{ac(cos)}\Delta T \sin 2a]/\{1 \\ &+ \mathrm{dc(cos)}(\mathrm{LD}/2) \sin 2\beta \\ &+ \Delta T[(\mathrm{LD}/2) \cos 2(a - \beta) \\ &+ \mathrm{dc(cos)} \sin 2a]\}. \end{aligned} \tag{A9}$$

Using the values dc(cos) = 0.32 and $\Delta T = 0.05$ (see the text), we have, within 1–2% uncertainty,

$$\begin{aligned} I_{ac}/I_{dc} = [&\mathrm{ac(cos)}(\mathrm{LD}/2) \sin 2\beta \\ &+ \mathrm{ac(cos)}\Delta T \sin 2a]/[1 \\ &+ \mathrm{dc(cos)}\Delta T \sin 2a]. \end{aligned} \tag{A10}$$

If one superposes an LD on a sample of CD, one obtains a total photodetector output

$$\begin{aligned} I(\mathrm{LD} + \mathrm{CD}) = I_{dc} + I_{ac} &= 1 \\ &+ e^{\mathrm{LD}} + \cos \delta (e^{\mathrm{LD}} - 1) \sin 2\beta \\ &+ 2 \tanh (\mathrm{CD}/2) \sin \delta e^{\mathrm{LD}/2} \\ &+ \Delta T \operatorname{sech} (\mathrm{CD}/2)[(e^{\mathrm{LD}} - 1) \\ &\cdot \cos (2\beta - \mathrm{CB} - 2a) \\ &- 2e^{\mathrm{LD}/2} \cos \delta \cos 2\beta \sin \\ &\cdot (2\beta - \mathrm{CB} - 2a) \\ &+ (e^{\mathrm{LD}} + 1) \cos \delta \sin 2\beta \cos \\ &\cdot (2\beta - \mathrm{CB} - 2a)], \end{aligned} \tag{A11}$$

where CB is the circular birefringence accompanying the CD. Because CD ~ CB ~ 10^{-4} in our case, the same numerical approximations leading to Eq. A10 gives

$$\begin{aligned} I_{ac}/I_{dc} = [&\mathrm{ac(sin)}\mathrm{CD}/2 + \mathrm{ac(cos)}(\mathrm{LD}/2) \sin 2\beta \\ &+ \mathrm{ac(cos)}\Delta T \sin 2a]/[1 + \mathrm{dc(cos)}\Delta T \sin 2a]. \end{aligned} \tag{A12}$$

We now consider a combination of LD_1 + LB + CD + CB + LD_2 like our multilayer samples, where LB is linear birefringence. We shall derive our results in three steps. First, using only the approximations tanh CD = CD, tanh LD_1 = LD_1, and tanh LD_2 = LD_2, we have the total photodetector output

$$\begin{aligned} I(\mathrm{LD}_1 + \mathrm{LB} + \mathrm{CD} + \mathrm{CB} + \mathrm{LD}_2) = I_{dc} + I_{ac} &= 1 \\ &+ (\mathrm{CD}/2)(\cos 2\beta \sin \mathrm{LB} \cos \delta + \cos \mathrm{LB} \sin \delta) \\ &+ (\mathrm{LD}_1/2) \sin 2\beta \cos \delta - (\mathrm{LD}_2/2)[1 - \cos \mathrm{CB} \sin 2\beta \\ &\cdot \cos \delta - \sin \mathrm{CB}(\cos 2\beta \cos \mathrm{LB} \cos \delta - \sin \mathrm{LB} \sin \delta)] \\ &+ \Delta T[\cos (\mathrm{CB} + 2a - 2\beta) \sin 2\beta \cos \delta + \sin \\ &\cdot (\mathrm{CB} + 2a - 2\beta)(\cos 2\beta \cos \mathrm{LB} \cos \delta - \sin \mathrm{LB} \sin \delta)] \\ &- (\mathrm{CDLD}_2/4)(\cos 2\beta \sin \mathrm{LB} \cos \delta + \cos \mathrm{LB} \sin \delta) \\ &+ (\mathrm{LD}_1\mathrm{LD}_2/4) \cos \mathrm{CB} - \Delta T(\mathrm{LD}_2/2) \cos 2(a - \beta) \\ &+ \Delta T(\mathrm{LD}_1/2) \cos (\mathrm{CB} + 2a - 2\beta) \\ &+ \Delta T(\mathrm{LD}_1\mathrm{LD}_2/4) \cos 2(a - \beta) \cos 2\beta \cos \delta \\ &- \Delta T(\mathrm{CDLD}_2/4) \cos 2(a - \beta)(\cos 2\beta \sin \mathrm{LB} \cos \delta \\ &+ \cos \mathrm{LB} \sin \delta). \end{aligned} \tag{A13}$$

Second, we neglect the last six terms and put CB equal to zero in Eq. A13. This is based on the orders of magnitude characteristic of our samples: CD ~ CB ~ 10^{-4}, LD_1 ~ LD_2 ~ 4×10^{-3} (also $\Delta T \sim 0.05$). In making these approximations, we note that the dc terms are compared

with 1, whereas the ac terms are compared with CD ~ 10^{-4}. The error caused by these approximations is <1%. The result is

$$I = 1 + (CD/2)(\cos 2\beta \sin LB \cos \delta + \cos LB \sin \delta) + [(LD_{1+}LD_2)/2] \sin 2\beta \cos \delta + \Delta T \sin 2a \cos \delta - \Delta T \sin 2(a - \beta) \sin LB \sin \delta + \Delta T (\cos LB - 1) \cos \delta \cdot [\sin 2a \cos^2 2\beta - (1/2) \cos 2a \sin 4\beta]. \quad (A14)$$

The third step consists of more detailed quantitative analysis. We examine the dc terms first. In the text we show that $1 - \cos LB \leq 0.03$. With dc(sin) < 10^{-3} (Shindo and Nakagawa, 1985) and the orders of magnitude of CD, LD, and ΔT given above, we see that I_{dc} is the same as in the previous cases (Eqs. A7, A10, and A12), i.e.,

$$I_{dc} = 1 + dc(cos)\Delta T \sin 2a, \quad (A15)$$

with <1% error. Thus, the apparent CD separates into two parts:

$$I_{ac}/I_{dc} = (I_{ac}/I_{dc})_1 + (I_{ac}/I_{dc})_2, \quad (A16)$$

$$(I_{ac}/I_{dc})_1 = [ac(sin)/2I_{dc}]CD \cos LB + [ac(cos)\Delta T \sin 2a/I_{dc}][1 - (1 - \cos LB) \cos^2 2\beta], \quad (A17)$$

$$(I_{ac}/I_{dc})_2 = (2I_{dc})^{-1}[ac(cos)CD \sin LB \cos 2\beta + ac(cos)(LD_{1+}LD_2) \sin 2\beta + ac(sin)2\Delta T \sin LB \sin 2(\beta - a) + ac(cos)\Delta T(1 - \cos LB) \cos 2a \sin 4\beta]. \quad (A18)$$

The first part consists of the CD signal and the baseline, whereas the second part can be removed by averaging over β, as discussed in the text.

We thank Wenhan Liu for helpful discussions on the CD instrumentation.

This research was supported in part by the Office of Naval Research Contract No. N00014-86-K-0087, the Robert A. Welch Foundation, and the National Institutes of Health Biophysics Training Grant GM08280.

Received for publication 25 May 1989 and in final form 20 November 1989.

REFERENCES

Born, M., and E. Wolf. 1980. Principles of Optics. Pergamon Press, New York. 670–681.

Dittmer, J. D., and M. A. Wells. 1969. Quantitative and qualitative analysis of lipids and lipid components. *Methods Enzymol.* 14:482–530.

Fasman, G. D. 1974. Optical rotatory dispersion. *Methods Enzymol.* 6:931–957.

Huang, H. W., and G. A. Olah. 1987. Uniformly oriented gramicidin channels embedded in thick monodomain lecithin multilayers. *Biophys. J.* 51:989–992.

Imahori, K., and N. A. Nicola. 1973. Optical rotatory dispersion and the main chain conformation of proteins. *In* Physical Principles and Techniques of Protein Chemistry. S. J. Leach, editor. Academic Press, New York. 357–444.

Mandel, R., and G. Holzwarth. 1972. Circular dichroism of oriented helical polypeptides: the alpha-helix. *J. Chem. Phys.* 57:3469–3477.

Moffitt, W. 1956. Optical rotatory dispersion of helical polymers. *J. Chem. Phys.* 25:467–478.

Moffitt, W., D. D. Fitts, and J. G. Kirkwood. 1957. Critique of the theory of optical activity of helical polymers. *Proc. Natl. Acad. Sci. USA.* 43:723–730.

Nagaraj, R., and P. Balaram. 1981. Conformations of synthetic alamethicin fragments. Evidence for 3_{10} helical folding from 270-MHz Hydrogen-1 nuclear magnetic resonance and circular dichroism studies. *Biochemistry.* 20:2828–2835.

Olah, G. A., and H. W. Huang. 1988*a*. Circular dichroism of oriented α helices. I. Proof of the exciton theory. *J. Chem. Phys.* 89:2531–2537.

Olah, G. A., and H. W. Huang. 1988*b*. Circular dichroism of oriented α-helices. II. Electric field oriented polypeptides. *J. Chem. Phys.* 89:6956–6962.

Schellman, J., and H. P. Jensen. 1987. Optical spectroscopy of oriented molecules. *Chem. Rev.* 86:1359–1399.

Shindo, Y., and M. Nakagawa. 1985. Circular dichroism measurements. I. Calibration of a circular dichroism spectrometer. *Rev. Sci. Instrum.* 56:32–39.

Shindo, Y., and Y. Ohmi. 1985. Problems of CD spectrometers 3. Critical comments on liquid crystal induced circular dichroism. *J. Am. Chem. Soc.* 107:91–97.

Tinoco, I., Jr., 1964. Circular dichroism and rotatory dispersion curves of helices. *J. Am. Chem. Soc.* 86:297–298.

Tinoco, I., Jr., and W. G. Hammerle. 1956. The influence of an external electric field on the optical activity of fluids. *J. Phys. Chem.* 60:1619–1623.

Tunis-Schneider, M. J. B., and M. F. Maestre. 1970. Circular dichroism spectra of oriented and unoriented deoxyribonucleic acid films—A preliminary study. *J. Mol. Biol.* 52:521–541.

Velluz, L., M. Legrand, and M. Grosjean. 1965. Optical circular dichroism. Academic Press, New York. 57–60.

Woody, R. W. 1968. Improved calculation of the $n\pi^*$ rotational strength in polypeptides. *J. Chem. Phys.* 49:4797–4806.

Woody, R. W. 1985. Circular dichroism of peptides. *In* The Peptides. S. Udenfriend and J. Meienhofler, editors. Academic Press, New York. 15–114.

Yamaoka, K., K. Ueda, and I. Kosako. 1986. Far-ultraviolet electric linear dichroism of poly(γ-methyl-L-glutamate) in Hexafluoro-2-propanol and the peptide band in the 187–250 nm wavelength region. *J. Am. Chem. Soc.* 108:4619–4625.